Supporting Online Material for

The Southern Ocean Biological Response to Aeolian Iron Deposition

Nicolas Cassar,* Michael L. Bender, Bruce A. Barnett, Songmiao Fan, Walter J. Moxim, Hiram Levy II, Bronte Tilbrook

*To whom correspondence should be addressed. E-mail: ncassar@princeton.edu

Published 24 August, *Science* **317**, 1067 (2007)
DOI: 10.1126/science.1144602

This PDF file includes:

Supporting Online Material

Materials and Methods

Measurements

The discrete O_2/Ar sample collection and laboratory analyses were performed as described in Hendricks et al. (*1*) and Reuer et al (*2*). See Hendricks et al. (*1*) for a detailed description of calculations and analytical uncertainties. We define NCP as gross photosynthesis minus auto- and hetero-trophic respiration, where gross photosynthesis is the rate of photochemical oxidation of water at photosystem II (PSII) of the photosynthetic apparatus. We partition our samples into hydrographic zones of the Antarctic (*3*) and according to sampling season over the austral Fall (March to May), Spring (September to November) and Summer (December to February) seasons. We then average values of NCP and GPP by zone and season.

Biological O_2 supersaturation is calculated from the ratio of the O_2/Ar ratio to the equilibrium value, and is defined as:

$$\text{Biological } O_2 \text{ supersaturation} = [\frac{(O_2 / Ar)_{meas}}{(O_2 / Ar)_{sat}} - 1]x100 \qquad (1)$$

$(O_2/Ar)_{meas}$ and $(O_2/Ar)_{sat}$ are the measured and saturated dissolved gas ratios, respectively (*4*). Ar measurements allow us to subtract out that portion of O_2 supersaturation due to the physical processes of warming and bubble entrainment (*5*, *6*).

O_2 NCP is inferred from biological O_2 supersaturation and the gas exchange coefficient (parameterized in terms of windspeed):

$$NCP = k \cdot [O_2]_{sat} \cdot \rho \cdot \text{Biological } O_2 \text{ supersaturation} \cdot 10^{-2} \quad (1)$$

where $[O_2]_{sat}$, k and ρ are the saturation O_2 concentration, the piston velocity (m d^{-1}), and seawater density, respectively. Most of the uncertainty associated with NCP measurements stems from estimates of the gas exchange coefficient (*7*), which here are based on the quadratic relationship of Wanninkhof (*8*). The O_2 concentration at a given time is dependent on the biological and physical (e.g. mixed-layer thickness and wind speed) history of the mixed-layer. To calculate k, we determine the history of piston velocities for 60 days prior to sample collection. A weighted average is then calculated by discounting a given day's value according to the extent of mixed-layer flushing between that day and the date of sample collection (*7*).

A weighting method on piston velocity estimates, derived from 60 day NCEP/NCAR wind speed reanalysis (*9*), is used to account for wind speed variability history prior to discrete sample collections. MLDs were estimated by linear interpolation of the models' estimates to our sampling sites and dates. Climatological MLD are based on Kara et al. (*10*).

GPP

Most processes fractionate oxygen isotopes in a mass-dependent mode. Stratospheric photochemical reactions fractionate oxygen isotopes anomalously relative to mass-dependent predictions (*11*). GPP estimates are based on the triple isotope composition of dissolved O_2. $\delta^{17}O$ of photosynthetic O_2 is nominally equal to 0.516 $\delta^{18}O$, whereas $\delta^{17}O$ of atmospheric O_2 deviates from 0.516 $\delta^{18}O$. The relation between $\delta^{17}O$ and $\delta^{18}O$ in dissolved O_2 is therefore a function of the antagonistic influences of

atmospheric exchange and gross photosynthesis (*1*, *12*, *13*). The anomalous isotopic signature, $^{17}\Delta$ (in per meg), is defined as:

$$^{17}\Delta = [\ln(\delta^{17}O/10^3 + 1) - 0.516 \ln(\delta^{18}O/10^3 + 1)]\, 10^6 \quad (2)$$

where the scalar "0.516" is the expected mass dependent fractionation associated with respiration (*14*). As opposed to gas exchange, photosynthesis increases $^{17}\Delta$. $^{17}\Delta$ of photosynthetically sterile water at equilibrium with the atmosphere is 8 per meg ($^{17}\Delta_{sat}$). Gross photosynthesis increases this value, up to 249 per meg, in which case the oxygen present in the water is entirely derived from photochemical oxygen evolution at PSII ($^{17}\Delta_w$). One calculates GPP as the rate of photosynthetic O_2 production required to maintain the observed deviation of $\delta^{17}O$ (defined as $^{17}\Delta \approx \delta^{17}O - 0.516 \cdot \delta^{18}O$) from the value in equilibrium with air (*1*):

$$GPP = k \cdot [O_2]_{sat} \cdot \frac{(^{17}\Delta_{sat} - ^{17}\Delta_{meas})}{(^{17}\Delta_{meas} - ^{17}\Delta_w)} \quad (3)$$

where $^{17}\Delta_{meas}$ is the composite isotopic signature of the sample.

Statistical Analysis

An analysis of average Fe deposition 28, 21, 14, 7, and 3 days prior to our observations shows the strongest correlation when 14 days of Fe deposition are included in the comparison (r_{28},r_{21},r_{14}, r_7, r_3 equal to 0.47, 0.48, 0.53, 0.34, 0.14, respectively). Synoptic hereafter refers to 14 day average Fe deposition. If we assume that Fe deposition and NCP follow a bivariate normal distribution, a significance test with the null hypothesis that synoptic Fe deposition and NCP are uncorrelated ($\rho=0$) is rejected at $p<0.01$ (Pearson correlation coefficient $r=0.53$, DF=381). Non-parametric Kendall and

Spearman analyses also show, with better than 99% confidence, that the correlation is significant (r_s=0.54 and τ=0.38, respectively). The correlation of NCP to annual (year of collection and decadal-1995-2004 average Fe deposition rate) Fe deposition estimates are also significant (0.60 and 0.49, respectively, DF=381) and similar in magnitude to the correlation with synoptic Fe deposition estimates. The dependence of GPP on Fe deposition is also significant ($p<0.01$). Averaging our NCP measurements by region (i.e., area between fronts) decreases the proportion of unexplained variation ($R^2 = 0.92$). Regional estimates of GPP also show a correlation to synoptic aeolian Fe deposition (R^2=0.74). As revealed by the NCP correlation coefficients to Fe and dust deposition, the inclusion of atmospheric Fe chemistry in the dust transport model significantly improves the correlation to our NCP estimates (e.g., r_{Fe}=0.53 vs. r_{Dust}=0.33 for the case of the synoptic timescale). The correlation between summer NCP measurements and corresponding average climatological photosynthetic active radiation within the mixed-layer is not significant (r=-0.0059, DF=371). The latter is based on an optical model (*15*) with SeaWIFS climatological ocean surface PAR and chlorophyll (*16*) and ECCO ocean data assimilation mixed-layer depth estimates (*17*).

Atmospheric Fe deposition model

The dominant source of atmospheric Fe is dust particles entrained into the atmosphere by desert windstorms. Chemical reactions in dust particles during atmospheric transport can lead to acid coating and subsequent dissolution of ferric Fe minerals (hematite/goethite). Dust particles are transferred from the atmosphere to the ocean by precipitation scavenging and surface dry deposition. The deposition flux of Fe is calculated in the Geophysical Fluid Dynamics Laboratory Global Chemical Transport

Model (GFDL/GCTM). The GCTM uses winds and other meteorological fields derived from NCEP reanalysis. The model has 28 vertical levels, and equal-area horizontal grids at a 265 km resolution, with subgrid-scale mixing parameterized based on vertical wind shear and stability. Vertical velocities are calculated from the horizontal mass divergence and the surface pressure tendency. The emission flux of dust particles is parameterized based on wind speed or friction velocity, with a threshold below which no emission occurs. Processes for wet deposition of dust particles in the model include ice and droplet nucleation, and below-cloud scavenging. Dry deposition is parameterized based on dust size and wind speed. Dust particles are also transported downward by gravitational sedimentation, and precipitation with subsequent re-evaporation of rain drops and ice particles.

Three types of dust tracer are carried in the GCTM to separate the three life stages of dust particles: fresh, coated and dissolved (for Fe). Dust particles are emitted as fresh. Dust mass is transferred from fresh to coated through chemical reactions with HNO_3 and SO_2 molecules, and through cloud processing (scavenging by cloud drops followed by evaporation of water), and subsequently to dissolved at a constant rate. The mass of each type is distributed in four size bins (0.1-1, 1-1.8, 1.8 3, and 3-6 micrometers in radius). The solubility of aerosol Fe is assumed to be 1% in the fresh and coated types and 100% in the dissolved type in this two-step parameterization. Not included in the model are variations in Fe solubility due to changes in source regions. Additionally, the potentially important process of atmospheric photoreductive Fe solubilization is not taken into account explicitly (*18*).

The conclusions reported here are dependent on the GFDL/GCTM model simulation of soluble Fe flux in the southern hemisphere. Unfortunately, there are no direct measurements available of soluble Fe flux to the oceans. However, there are measurements of percent Fe solubility, mineral dust concentrations and mineral dust deposition, albeit sparse in the southern hemisphere. The model of Fan et al. (*19*) agrees qualitatively well with the numerous percent Fe solubility observations in the northern hemisphere and tropics, providing support that the same physical processes, transport and Fe deposition should apply to the southern hemisphere. Overall, we find that the agreement of the model's predictions to observations in the Southern Ocean is similar to other areas of the world's oceans. Below we present the available southern hemisphere observations of mineral dust concentration, deposition, and percent Fe solubility.

Figure S4 compares model and observed dust (Al) concentrations at Cape Grim (40.7^{o}S, 144.7^{o}E), King George Island (62.2^{o}S, 58.3^{o}W), and Neumayer Station (70.6^{o}S, 8.4^{o}W) (*20, 21*). Dust concentrations range from about 1.5 μg/m^3 at Cape Grim to about 0.5 μg/m^3 at King George Island and 0.01 μg/m^3 at Neumayer Station. Model results are within a factor of 2 of the measurements. While the model captures the strong poleward gradient (2 orders of magnitude), it does not consider the effect of soil moisture on dust emission which affects seasonal variability.

Model-simulated dust-deposition fluxes compare reasonably well with the few available sediment trap measurements of lithogenic particle flux (Table S1). There are many factors that could obscure a relationship between the modeled fluxes of dust and the trap measurements. The traps are prone to undertrapping in high current

regimes, lateral advection of particles can alter trap collections, and interannual variability, combined with strong meridional gradients in the fluxes (*22, 23*), make direct comparisons with the modeled fluxes difficult.

The model simulated aerosol Fe solubility is 10-15% in the Southern Ocean near Antarctica, and >20% over Antarctica, while measurements of Fe solubility in snow average to 32% (range 10-90%) (*24*). We cannot however rule out that Fe solubility may increase by photo-reduction in aged snow samples. Aerosol Fe solubility measured in the South Atlantic is on average 9% (range 4-17%) (*25*), compared to 12% (range 1-22%) for the model. It should be noted that soluble Fe is operationally defined as the fraction of Fe in melt water passing through 0.4 μm filters, which includes particulate Fe less than 0.4 μm in size.

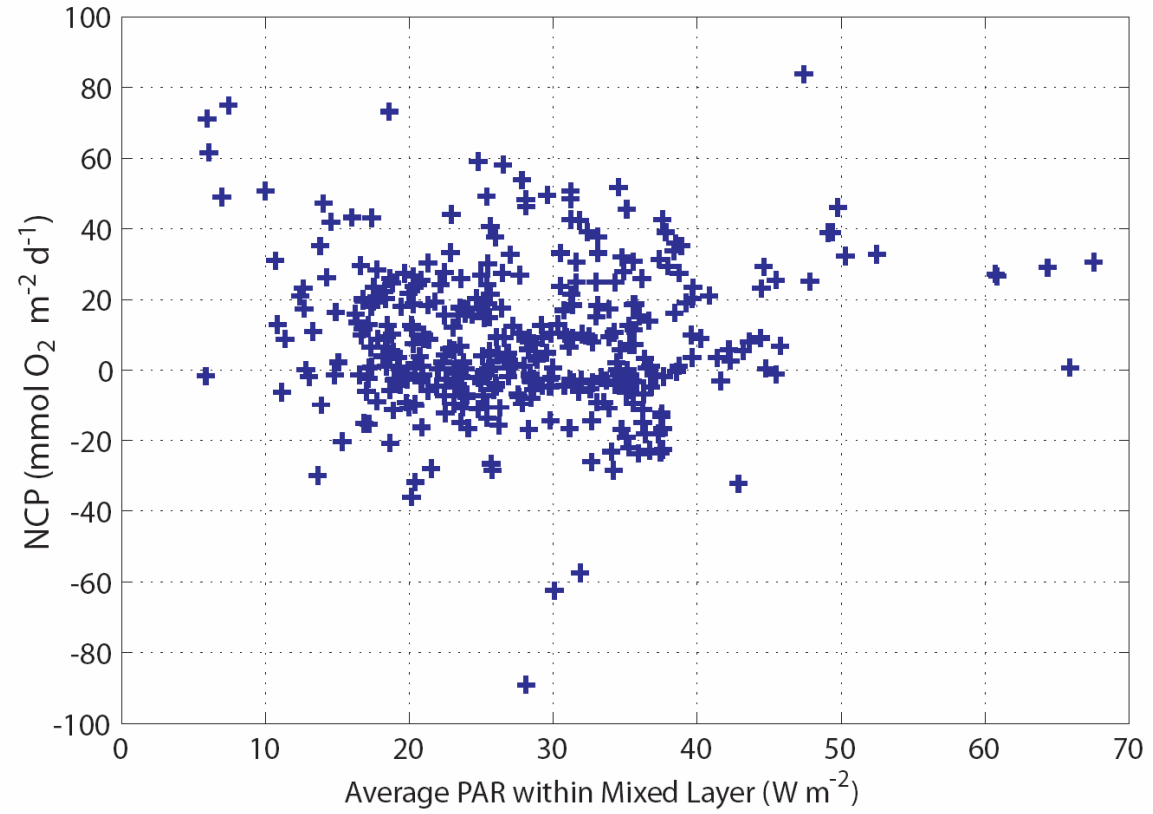

Figure S1. Summer NCP vs. vertically averaged climatological PAR within Mixed layer.

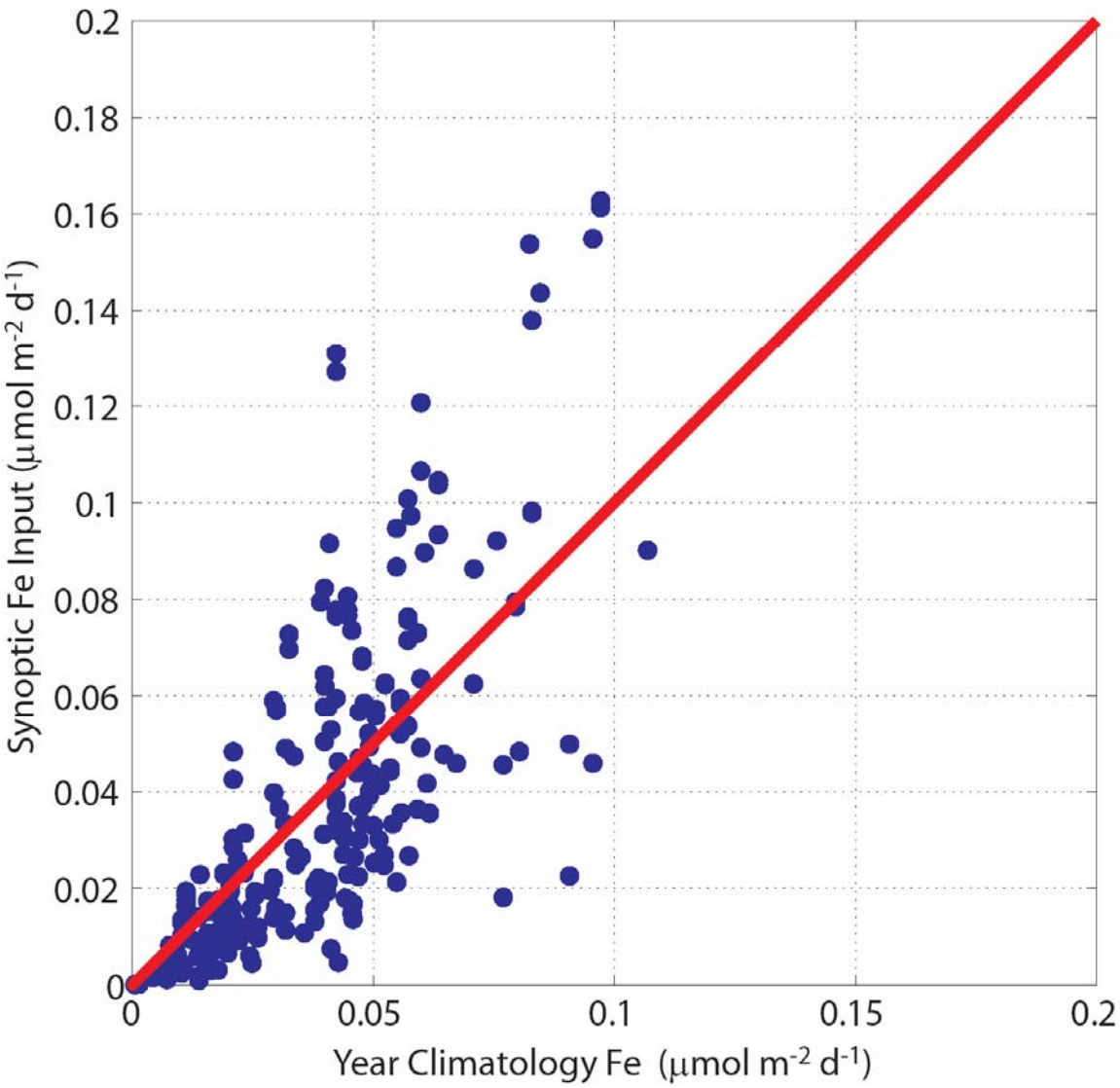

Figure S2. Average Fe deposition at sampling sites during the 2 week period prior to collection vs. average annual Fe deposition at the sites.

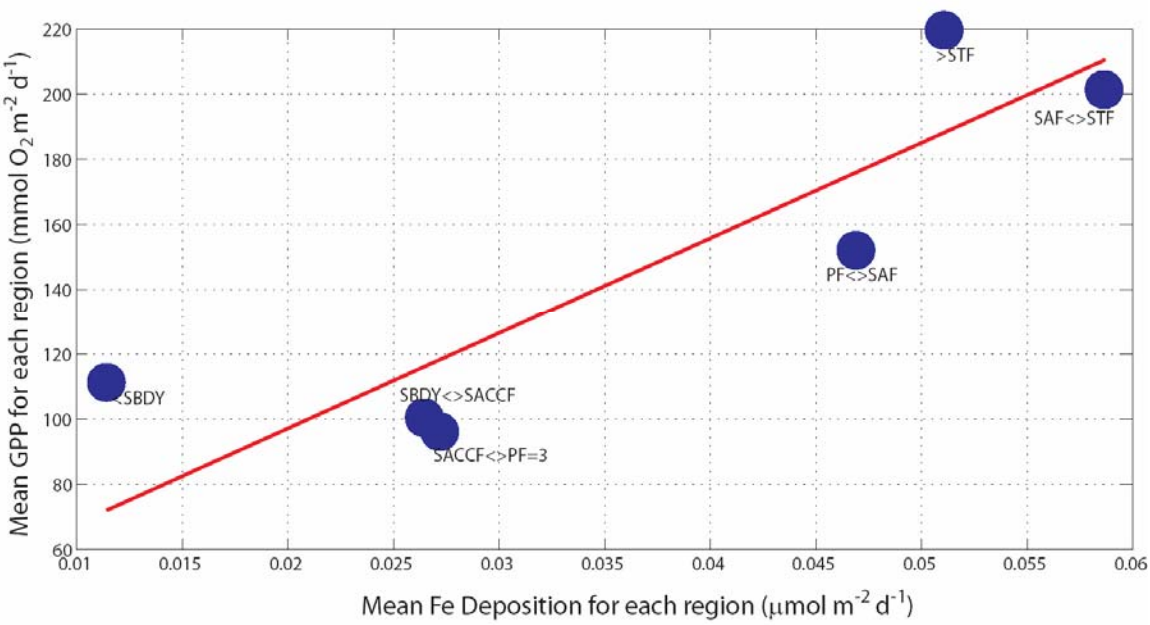

Figure S3. Regional mean GPP vs. regional mean synoptic Fe deposition

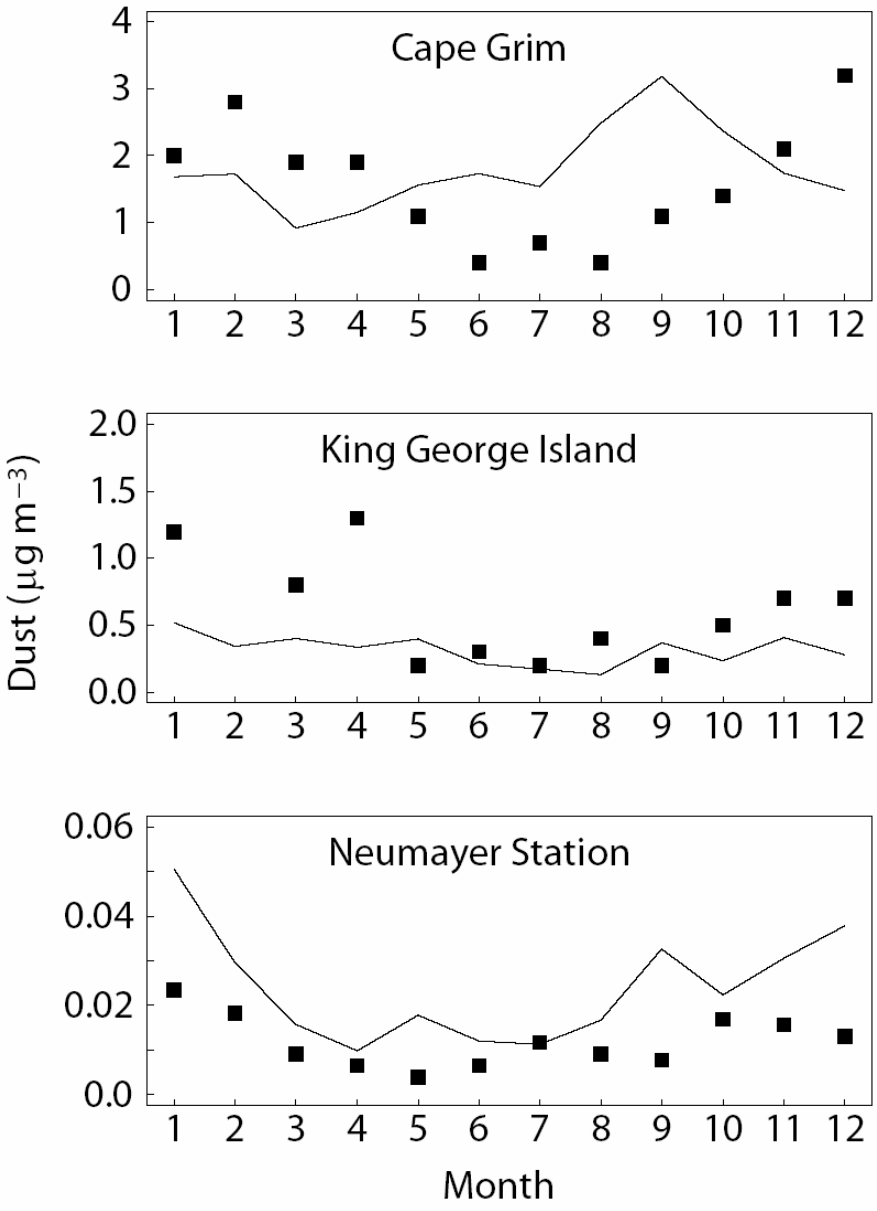

Figure S4. Model and observed dust concentrations at several stations south of 40°S.

Site	Lat	Lon	Obs.	Model (1994-1998)	Model (1994-2004)	Obs. Source
M8101-38m	60.9°S	57.1°W	1.08	0.84	1.15	Wefer et al., 1982 (*26*)
MS-5	66.2°S	169.7°W	0.05	0.09	0.09	Honjo et al., 2000 (*23*)
MS-4	63.2°S	169.9°W	0.12	0.15	0.16	
MS-3	60.3°S	170.0°W	0.12	0.21	0.21	
MS-2	56.9°S	170.2°W	0.12	0.23	0.23	
MS-1	53.0°S	174.7°W	0.73	0.39	0.39	
47_2000	47.0°S	142.0°E	0.66	1.07	1.09	Trull et al., 2001 (*22*)
51_3100	51.0°S	142.0°E	0.28	0.79	0.89	
54_1500	54.0°S	142.0°E	0.06	0.36	0.45	

Table S1. Model predictions vs. various sediment trap derived dust deposition flux estimates (g m^{-2} yr^{-1}) in the Southern Ocean.

References

S1. M. B. Hendricks, M. L. Bender, B. A. Barnett, *Deep-Sea Research Part I-Oceanographic Research Papers* **51**, 1541 (2004).

S2. M. K. Reuer, B. A. Barnett, M. L. Bender, P. G. Falkowski, M. B. Hendricks, *Deep-Sea Research I* **54**, 951 (2007).

S3. A. H. Orsi, T. Whitworth, W. D. Nowlin, *Deep-Sea Research Part I-Oceanographic Research Papers* **42**, 641 (May, 1995).

S4. H. Craig, T. Hayward, *Science* **235**, 199 (Jan 9, 1987).

S5. S. Emerson, *Journal of Geophysical Research-Oceans* **92**, 6535 (Jun 15, 1987).

S6. W. S. Spitzer, W. J. Jenkins, *Journal of Marine Research* **47**, 169 (Feb, 1989).

S7. M. K. Reuer, B. A. Barnett, M. L. Bender, P. G. Falkowski, M. B. Hendricks, *Deep-Sea Research II* (in press).

S8. R. Wanninkhof, *Journal of Geophysical Research-Oceans* **97**, 7373 (May 15, 1992).

S9. E. Kalnay *et al.*, *Bulletin of the American Meteorological Society* **77**, 437 (Mar, 1996).

S10. A. B. Kara, P. A. Rochford, H. E. Hurlburt, *Journal of Geophysical Research-Oceans* **108** (Mar 13, 2003).

S11. M. H. Thiemens, *Science* **293**, 226 (Jul 13, 2001).

S12. B. Luz, E. Barkan, *Science* **288**, 2028 (Jun 16, 2000).

S13. L. W. Juranek, P. D. Quay, *Global Biogeochemical Cycles* **19** (Jul 29, 2005).

S14. A. Angert, S. Rachmilevitch, E. Barkan, B. Luz, *Global Biogeochemical Cycles* **17**, 1089 (Mar 25, 2003).

S15. A. Morel, *Journal of Geophysical Research-Oceans* **93**, 10749 (Sep 15, 1988).

S16. C. R. McClain, G. C. Feldman, S. B. Hooker, *Deep-Sea Research Part Ii-Topical Studies in Oceanography* **51**, 5 (2004).

S17. C. Wunsch, P. Heimbach, *Physica D* **in press**, doi:10.1016/j.physd.2006.09.040 (2006).

S18. J. L. Hand *et al.*, *Journal of Geophysical Research* **109** (2004).

S19. S. M. Fan, W. J. Moxim, H. Levy, *Geophysical Research Letters* **33** (Apr 7, 2006).

S20. C. Piel, "Variability of chemical and physical parameters of aerosol in the Antarctic troposphere" (2004).

S21. C. S. Zender, H. S. Bian, D. Newman, *Journal of Geophysical Research-Atmospheres* **108** (Jul 23, 2003).

S22. T. W. Trull, S. G. Bray, S. J. Manganini, S. Honjo, R. Francois, *Journal of Geophysical Research-Oceans* **106**, 31489 (Dec 15, 2001).

S23. S. Honjo, R. Francois, S. Manganini, J. Dymond, R. Collier, *Deep-Sea Research Part Ii-Topical Studies in Oceanography* **47**, 3521 (2000).

S24. R. Edwards, P. Sedwick, *Geophysical Research Letters* **28**, 3907 (Oct 15, 2001).

S25. A. R. Baker, T. D. Jickells, M. Witt, K. L. Linge, *Marine Chemistry* **98**, 43 (Jan 2, 2006).
S26. G. Wefer *et al.*, *Nature* **299**, 145 (1982).